Proceedings World Geothermal Congress 2020+1
Reykjavik, Iceland, April - October 2021

Establishing geothermometric constraints on the local geothermal gradients: case study of the eastern cordillera basin, Colombia.

Carlos A. Barrera [(1)], Carlos A. Vargas [(1)] and Jorge E. Cortes [(1.2.*)]

[(1)] Universidad Nacional de Colombia, Carrera 45 No 26-85 Bogotá, Colombia

[(2)] Petromarkers, Inc. 16850 Saturn Ln, Houston, TX 77058, United state

Correspondence to: Carlos A. Barrera (caabarrerala@unal.edu.co)

Keywords: geothermometers, hydrochemistry, coal bed, formation waters, Eastern Cordillera Basin.

ABSTRACT

Geochemical analyses were performed on 170 coal bed-trapped groundwater samples from 97 underground mines located in the Eastern Cordillera Basin, Colombia. The waters analyzed in this paper are from exploited coal beds, located up to 0.73 km deep, which emerge along with the local fault systems. The hydrochemical facies were classified based on the concentration of major ions by inferring the equilibrium state and rock water source. The main hydrochemical facies presented in the groundwater study are SO_4-Ca-Mg, HCO_3-Ca, HCO_3-Ca-Mg, and SO_4-HCO_3 mixed waters. We used geothermometric equations to estimate the most probable temperature under in-situ conditions and the propagation of errors theory to test the results. The geothermal gradient in the study area is close to 30 °C/km, which is consistent with measurements from oil wells within the study area. A Principal Component Analysis was used to explain factors affecting formation water composition and hydrogeochemical evolution of aquifers.

1. INTRODUCTION

Geothermics is a broad discipline in geophysics that deals with the theoretical study of the thermal regimes in the Earth, as well as engineering aspects using the Earth's natural heat. A relevant thermophysical parameter in this discipline is the geothermal gradient. This key piece of information is essential in the understanding of the thermal lithospheric structure and the thermal history of sedimentary basins, allowing for the evaluation of organic matter maturity and the generation of hydrocarbons. Also, it can be used to study the geothermal resources in a particular region. A widely used approach for geothermal gradient estimation is made by analyzing geochemical thermometers, which are empirical relations that correlate ion concentrations and temperatures at depths, and are based on the chemical balance between groundwater and local lithology (Díaz et al., 2008; Yock, 2009). However, in a sedimentary basin setting, geochemical thermometers are only applicable to scenarios where the pore water remains in a chemical equilibrium with the surrounding rocks, subject to in-situ temperature conditions.

There are gaps in knowledge regarding the behavior of these techniques when it comes to inferring the thermal structure of sedimentary basins which coexist with coal ore deposits, salt domes, and complex tectonic structures with current levels of orogenic activity. In this paper, we analyze the hydrogeological components and their relationship with the stratigraphic units of the Eastern Cordillera Basin in Colombia, in order to map thermal anomalies, and compare the results with well observations. We have estimated temperatures using chemical geothermometer, and have selected them on the basis of the propagation of errors theory. Consequently, the geothermal gradient is derived from the local stratigraphic record. The hydrogeochemical data has been used to generate maps and identify trends in the concentrations of Na, Ca, K, Mg, SO_4, HCO_3, CO_3, and Cl. Finally, a multivariate analysis was performed to evaluate the behavior of temperature as a function of the chemical components of the geothermometers used.

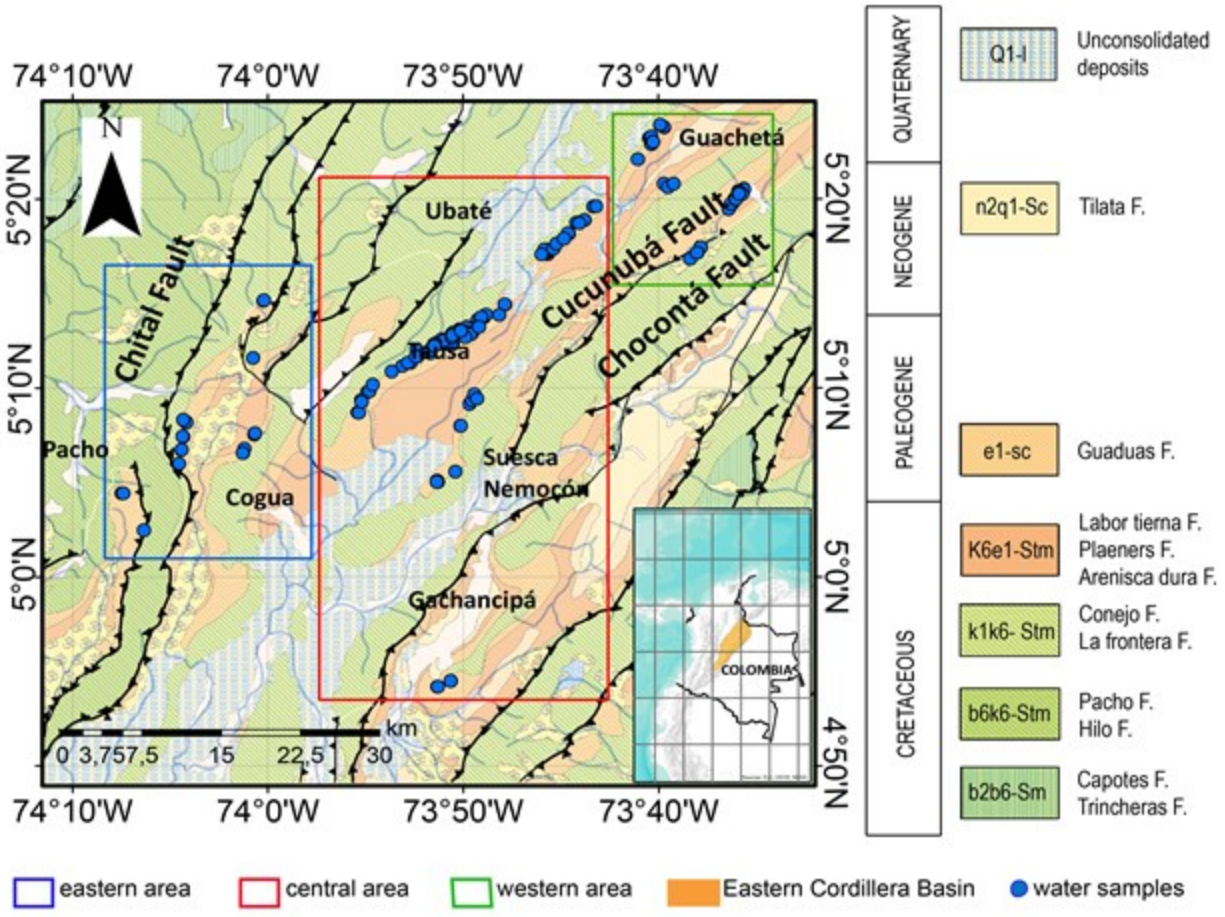

Figure 1: Geological setting of the Eastern Cordillera Basin, showing the major faults (indented black lines) and stratigraphic units. The blue circles represent locations sampled for the groundwater analyzed in this study, that are related to coal mines. The boxes indicate the three geographical areas where groundwater samples were collected. Geological units outcropping in the area correspond to sedimentary sequences of the Cretaceous to Quaternary period.

2. GEOLOGICAL SETTING

The Eastern Cordillera Basin (ECB) in Colombia constitutes rocks formed in an inverted Late Triassic rift system following the break-up of Pangea (Rolon et al., 2001), that are overlain by Mesozoic marine and Cenozoic continental sediments. Since the Early Paleogene, a dextral transpressional deformation, related to the Andean Orogeny, promoted the current structural inversion of the basin, with high thermal anomalies associated with the hydrothermal activity (Pedraza and Mariño, 2016). Coal beds in the basin are associated with the Guaduas Formation (Hubach, 1957), that were deposited in a transitional environment during the Late Cretaceous to Early Paleocene. Previous studies have described the stratigraphy of this unit as a mainly muddy succession with some sandy levels, characterized by containing several layers of coal (Sarmiento et al., 1994).

Figure 1 shows the study area, located west of the Eastern Cordillera Basin, Colombia. The structures in the area are dominated by the Cucunubá, Chital, and Choconta Faults. These are reverse faults with orientated mainly in the NE direction (Montoya and Reyes, 2003). Here, the coal beds occur in the Guaduas Formation, which were deposited in a coastal wetland and floodplain environment (Sarmiento, 2001). Figure 2 shows the lithostratigraphic column of the Eastern Cordillera Basin. Several authors have described the geology and hydrogeology of the study area (Montoya and Reyes, 2003; Etayo, 1968; Pérez and A Salazar, 1978; Fabre, 1985; Acosta and Ulloa, 1997; Guerrero, 2002). The Guaduas Formation comprises beds of claystone, coals, and sandstones. Palynological studies assign the Guaduas Formation to the Upper Maastrichtian-Lower Paleocene age (Sarmiento et al., 1992). In the study area, the Guaduas Formation is about 200 m thick (Guatame and Sarmiento, 2004).

Previous studies in the area have classified the coal as a high volatile bituminous A-type, in accordance with the Standard Classification of Coals, Rank ASTM D-388. The coals in this formation are dominated by macerals of the vitrinite group, with a lesser contribution of the inertinite and exinite groups. The mineral fraction corresponds to pyrite and clays minerals (Mejía et al., 2006).

Other units in the area (Figure 2) correspond to rocks of the Hilo Formation, a rock complex that includes shales, biomicrites, and diagenetic cherts that resulted from the replacement of biomicrite by silica (Etayo et al., 1979; Guerrero et al., 2000). Overlying this unit is the Pacho Formation, which constitutes mudstones and siltstones, with sporadic interbedding of sandstones, and a few horizons of grainstone/rudstone biosparites, and sandy biosparites (Ulloa, 1993). Caceres & Etayo (1969) defined the Frontera Formation to the Turonian strata composed of shales with calcareous concretions and beds of biomicrite, including thin beds of porcellanites and biogenic cherts. The Conejo Formation is made of mudstones and marlstones, with large Coniacian to Santonian calcareous

concretions and minor biomicrite and sandstone interbeds. The overlying Arenisca Dura Formation is a Campanian quartz sandstone of medium fine-grained and sandy mudstones. The Plaeners Formation (Hubach, 1951; Renzoni, 1963) includes "siliceous" siltstones and claystone, along with "lidites" and "porcellanites" fractured in cubic silica prisms. The unit includes phosphatic particles, fish spines and teeth, mud intraclasts, bioturbated strata and calcareous concretions with abundant pyrite and some ichnofossils (Guerrero and Sarmiento, 1996). The Labor Tierna Formation is usually used to group sandstones of fine-medium grained with occasional interleaves of mudstones layers with glauconitic and phosphate particles, and fish parts. The Labor Tierna Formation (Hubach, 1951) is composed of medium to coarse-grained quartz sandstones. Using thin section analysis, Pérez and A Salazar (1978) described the rocks as muddy sandstones of very fine to fine-grain size.

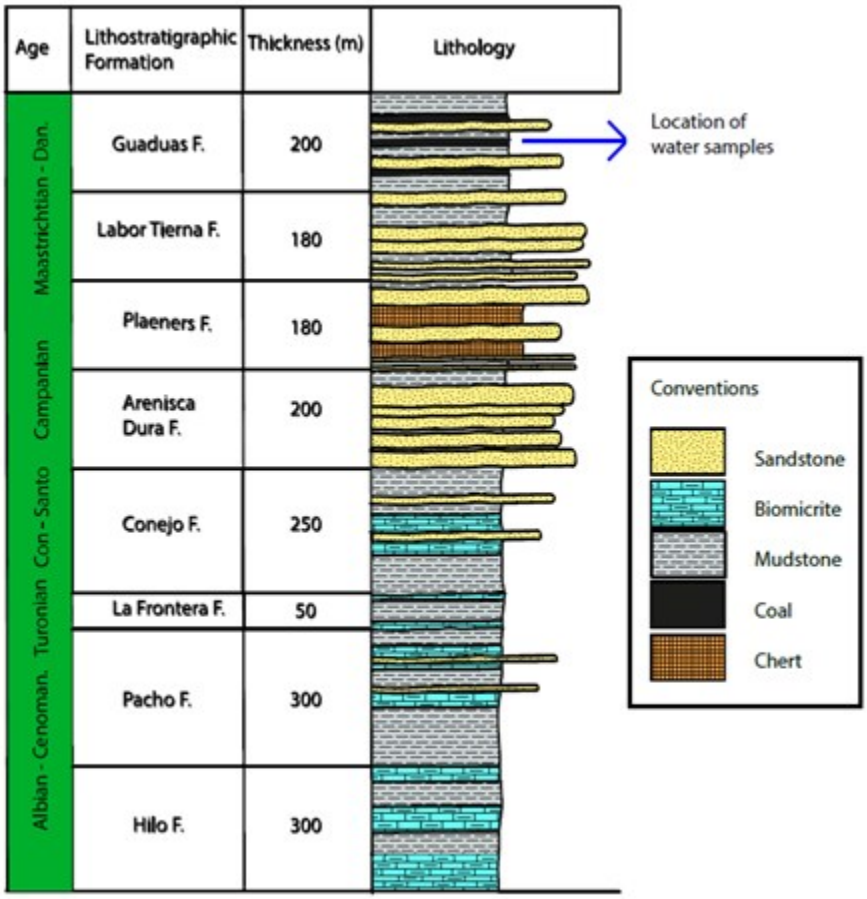

Figure 2: General lithostratigraphic column of the Eastern Cordillera Basin, Colombia. Modified after Guerrero (2002). The stratigraphic column shows the approximate thicknesses of the sedimentary sequences in the study area. Provenance of the groundwater is possibly related to units that underlie the Guaduas Formation. e.g., the Hilo, Pacho, La Frontera, Conejo, Arenisca Dura, Planers, and Labor Tierna Formations.

3. METHODOLOGY

One hundred and seventy groundwater samples were collected around the coal mines located in the Eastern Cordillera Basin between December 2014 and April 2015 (ANH-Antek, 2015). In-situ parameters including temperature, pH, electrical conductivity (EC), and total dissolved solids (TDS) were analyzed using a properly calibrated multi-parametric Hach D-660 instrument.

A 500 mL water sample was collected for major cation and metal analyses, and acidified to pH<2 using ultra-pure concentrated nitric acid. The Antek S.A.S-Environmental and Geochemical Laboratory ran all analyses including total and suspended solids, alkalinity, chloride, total calcium and magnesium hardness, carbonate, and bicarbonate, which were analyzed using gravimetric and titrimetric validation methods (Antek, 2009) based on U.S. EPA and Standard Methods (APHA, 2012). Sulfates were analyzed using a Thermo Scientific Spectrophotometer. The cations and major elements such as calcium, magnesium, sodium, potassium, and iron, were analyzed using a Perkin-Elmer 800 Atomic Absorption Spectrometer. The analytical precision, based on the ionic balance error, was < 10% (Prasanna et al., 2010; Chidambaram et al., 2012).

The Aquachem 5.1 hydrogeochemical software, version 2007-2008 from Waterloo Hydrogeologic (Waterloo Hydrogeologic, 2010) was used for the determination of geochemical correlations, graphics, ionic balance, dissolved minerals and other hydrogeochemical parameters. Concentration maps were modeled using the ArcGis-10.2 software (ESRI, 2010). A Multivariate Statistical Analysis was done using the XLStat software (Addinsoft, 2015). A Principal Component Analysis was used to explain the relationship between numerous variables, and establish the factors affecting formation water composition. The geothermeters were calculated based on concentrations of major ions (mg/l) using the SolGeo tool developed by Verma et al., (2008). A cluster analysis was carried out to investigate the similarities in each of the major ion concentrations using the median as the central measurement criterion (due to the asymmetrical probability function) (Abdel-Lattif et al., 2009; Brindhla et al., 2011).

The estimation of geothermometers requires a proper depth selection in the study area which guarantees a suitable fit for the current geological setting. Temperature estimations were derived from empirical relationships presented in Table 2. Concentrations in meq/L were converted to mg/l and replaced in these equations. We used previously reported relations as criterium for the selecting the best relation between ions and temperatures (Díaz et al., 2008; Verma P., 1997) based on the propagation of errors theory (Bevington, 2003).These mathematical relations were applied to the geothermometers using the variance provided with the original data used by authors to develop the equations relating to the analytical errors (see equations in Appendix A). For calculation of the geothermal gradient, we compared depths reported from the coal mines, where in-situ groundwater samples were collected, structural approximations made by previous authors (Acosta and Ulloa, 1997; Guatame and Sarmiento, 2004; Mejía et al., 2006) and estimations of the geothermal gradient as reported from two wells in the study area (Vargas, 2009).

Table 1:Physicochemical results for water samples in the Eastern Cordillera Basin. R.U. = Real Uncertainty. N.D. = Not Determined. The mean, median, S.D., and C.V. correspond to 73 samples in the eastern block, 101 samples in the central block, and 22 samples in the western blocks. A total of 170 samples were analyzed

	Eastern block				Central block				Western block				
	Mean	Median	S.D.	C.V.	Mean	Median	S.D.	C.V.	Mean	Median	S.D.	C.V.	R.U.
TEMP. (°C)	18.91	18.85	3.66	0.19	19.57	19.8	3.65	0.19	14.65	14.65	2.65	0.18	N.D.
Ph	6.62	6.94	0.85	0.13	6.84	7.18	1.51	0.22	6.82	7.11	0.85	0.13	N.D.
COND. (µS/cm)	761.19	322.75	662.69	0.87	1178.77	720	1498.41	1.27	555.6	442.15	421.08	0.76	0.023
Na (meq/L)	3.51	7.16	5.92	1.69	7.09	2.71	10.02	1.41	0.98	0.48	1.26	1.29	0.039
SO4 (meq/L)	3.38	2.7	6.39	1.89	10.32	4.96	18.8	1.82	4.73	1.85	6.52	1.38	0.021
HCO3 (meq/L)	3.16	4.44	3.39	1.07	3.24	2.45	2.8	0.86	1.96	0.67	2.15	1.1	0.0016
Cl (meq/L)	0.19	0.09	0.1	0.54	0.31	0.12	0.6	1.94	0.12	0.09	0.06	0.52	0.032
Mg (meq/L)	1.27	0.86	2.25	1.77	3.21	1.46	6.26	1.95	1.76	1.56	1.29	0.73	0.026
Ca (meq/L)	1.86	1.67	3.62	1.94	4.14	2.39	7.16	1.73	3.96	3.02	4.84	1.22	0.026
CO3 (meq/L)	0.13	0.13	N/A	N/A	0.25	0.13	0.45	1.79	0.13	0.13	0	0	0.148
K (meq/L)	0.06	0.06	0.03	0.54	0.08	0.07	0.05	0.64	0.04	0.04	0.02	0.54	1.6

4. ANALYTICAL RESULTS AND DISCUSSION

4.1 Samples and Physicochemical parameters

The groundwater chemical composition is a result of its interaction with the regional lithology, as well as the dissolution and balance of the ionic charge in the water column (Cortes et al., 2016). Thus, the geochemistry of groundwater reflects the complexity of its historical flow through several rock types under varying conditions of temperature, pressure, and physicochemical composition (Méndez, 2017).

Figure 1 displays the study area, which is divided into three geographic regions based on the location of the coal mines. Table 1 shows the physicochemical and ionic concentrations, mean, median, standard deviation, and coefficient of variation for each parameter measured in each of the three sectors throughout the Eastern Cordillera Basin.

The surface temperature, on average is 14.65–19.57 °C throughout the basin, with pH average values being slightly below neutrality (varying between 2.79 and 8.83) with a mean value of 6.8, indicating that some samples are influenced by the iron sulfite (pyrite) oxidation processes generated by mine acid drainage. The electrical conductivity has an asymmetrical probabilistic distribution, for which we take the median as a representative point. The central region has a value of 1178.77±0.023 µS/cm, which is consistent with

a higher salt content (high mineralization), while the eastern and western areas show median values of 322.75±0.023 µS/cm and 442.15±0.023 µS/cm, respectively, indicating presence of secondary mineralization.

Table 2: Empirical relationships and nomenclature used in the geothermometer estimation, based on ion concentrations (mg/L).

Emprical relationships	Formula
Na/K temperature (Tonami, 1980) TNKT80	$t(°C) = \frac{833}{0.780 + \log(\frac{Na}{K})} - 273.15$
Na/K temperature (Arnórsson-1, 1983) TNK2A83	$t(°C) = \frac{933}{0.993 + \log(\frac{Na}{K})} - 273.15$
K/Mg temperature (Fournier-2, 1991) TKM2F91	$t(°C) = \frac{1077}{4.003 + \log(\frac{K^2}{Mg})} - 273.15$
K/Mg temperature (Giggenbach, 1988) TKMG88	$t(°C) = \frac{4410}{14.00 + \log(\frac{K^2}{Mg})} - 273.15$
Na-K-Ca temperature (Fournier and Truesdell, 1973) TNKCF73M	$t(°C) = \frac{1647}{log\left(\frac{Na}{K}\right) + \beta\left[log\left(\frac{\sqrt{Ca}}{Na}\right) + 2.06\right] + 2.47} - 273.15.$ $\beta = \frac{4}{3} for t \leq 100°C$

Figure 3: shows the distribution of major ions (meq/L) throughout the Eastern Cordillera Basin. In general, the probabilistic distribution of ions are asymmetrical and skewed, therefore for such a case we prefer to obtain the median by comparing all the elements. The Sulfate concentrations with median values ranging between 1.85±0.021 meq/L in the western region, to 4.96±0.021 meq/L in the central area, show a dominance over bicarbonate and chloride, in the respective regions. Bicarbonate shows concentrations of around 4.44±0.0016 meq/L in the eastern region compared to the west (0.67±0.021 meq/L), which has a similar coefficient of variation (C.V.; see the Table 1). Chloride shows a median of 0.09±0.032 meq/L in the eastern and western blocks, ranging between 0.09 to 0.12 ±0.032 meq/L throughout the basin, with a lower C.V. of 0.55 in the eastern and western areas. The major concentration of sulfates is consistent with low pH values as a result of pyrite oxidation, leaching, and acid runoff and effluents from the coal mines (Cortes et al., 2017).

With a median of 7.16±0.039 meq/L, sodium values in the eastern area show higher concentrations compared to the western area where concentration values are close to 0.48±0.039 meq/L. Calcium values reach their maximum value in the western and central areas with median values of 3.02±0.026 and 2.39±0.026 meq/L, respectively. Potassium concentrations are high in the central area, with a median of 0.07±1.6 meq/L, and the highest magnesium values were observed in the central and western areas with a median of nearly 1.5±0.026 meq/L.

The above physicochemical characteristics suggest the classification of these groundwaters as mainly sulfated, with a significant contribution of magnesium-bicarbonate, calcium chloride, sodium bicarbonate, and calcium-magnesium-chloride mixed waters. A

negligible contribution from chlorides was observed from the entire basin.

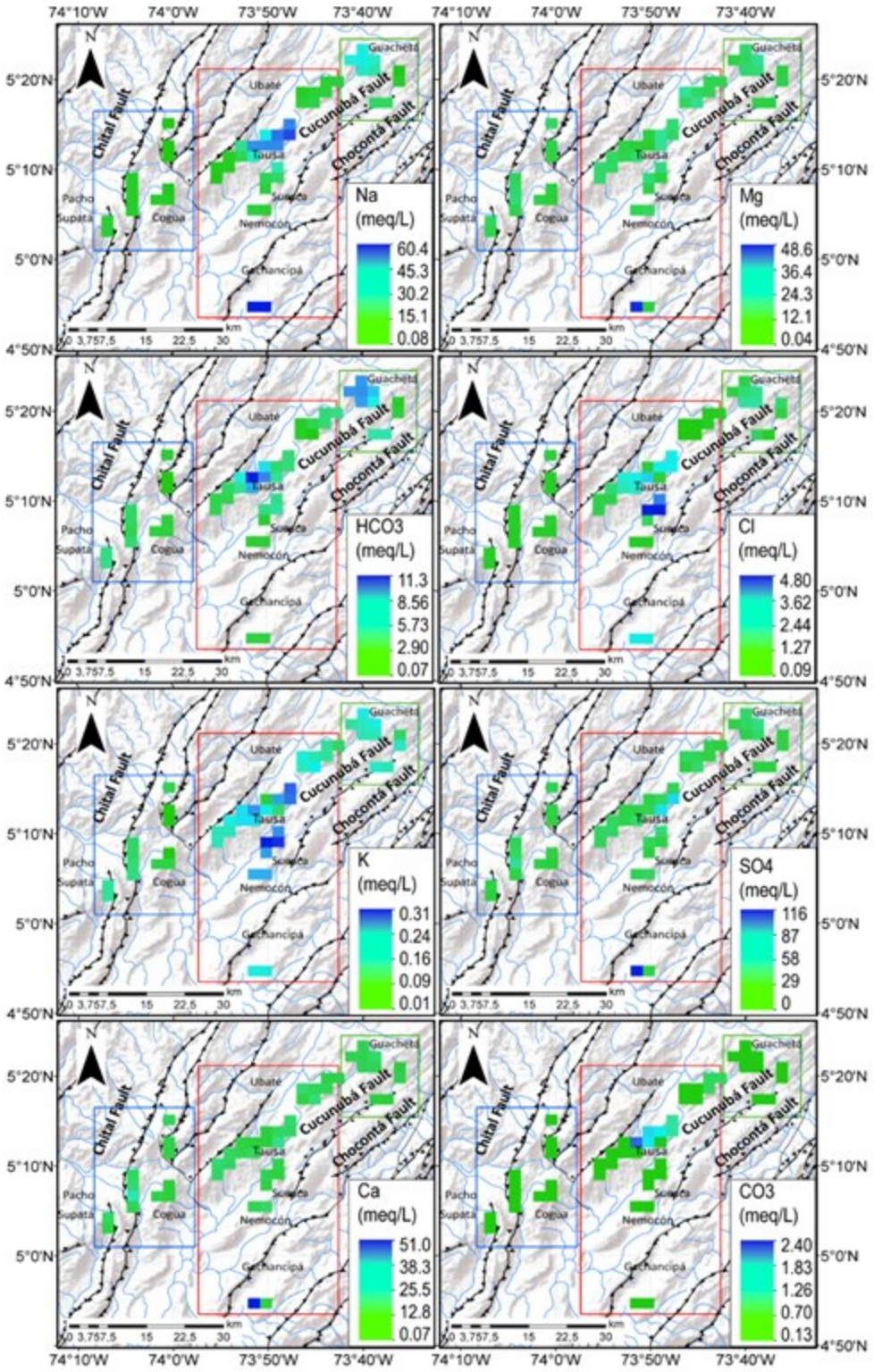

Figure 3: Major ions distribution (meq/L) in the Eastern Cordillera Basin, Colombia.

Figure 4a shows the piper diagram for the groundwater in the study area. The central diamond shaped field in the diagram shows that the groundwater, in most of the samples from the western area (blue circles), are of $MgSO_4$ type and $CaSO_4$ type, and in minor proportion, a combination of them. The eastern area samples (green circles) are mostly of the Na-SO_4-HCO_3, Mg-SO_4-HCO_3, and CaSO4 type, while in the central area (red circle), the samples are of multi-origins, covering all types of hydrochemical facies. The anion triangle indicates the dominance of SO_4 over HCO_3, with a very low concentration of chloride in the waters. In the cation triangle, an increment of the salinization from the eastern region towards the western, is seen.

The Giggenbach diagram is a geochemical plotting tool that allows observation of the rock-water equilibrium through a ternary relationship between Na, K, and Mg. The position of samples within the triangle allows sorting of sample waters into 'mature' or

'immature' types, and by its temperature in the reservoir. Immature waters fall close to the base of the triangle, or the triangle walls. Partially equilibrated waters fall in the center or between both curves, while the fully balanced (mature) waters are distributed above the upper curve (Cortes et al., 2016). Figure 4b indicates that set of samples are distributed between immature and partially equilibrated waters are from the western region, the eastern area samples are mostly of the immature type, and samples from the central area are partially equilibrated waters. The temperature of the groundwater samples can be evaluated using the Giggenbach diagram. In the eastern area, the estimated temperature is below 40 °C (cold waters), suggesting that the groundwater is probably mixed with a significant portion of meteoric waters altering its chemical composition (Bello et al., 2014; Hounslow, 1995).Samples from the central area show a broad range of temperatures varying between 40 °C and 120 °C.

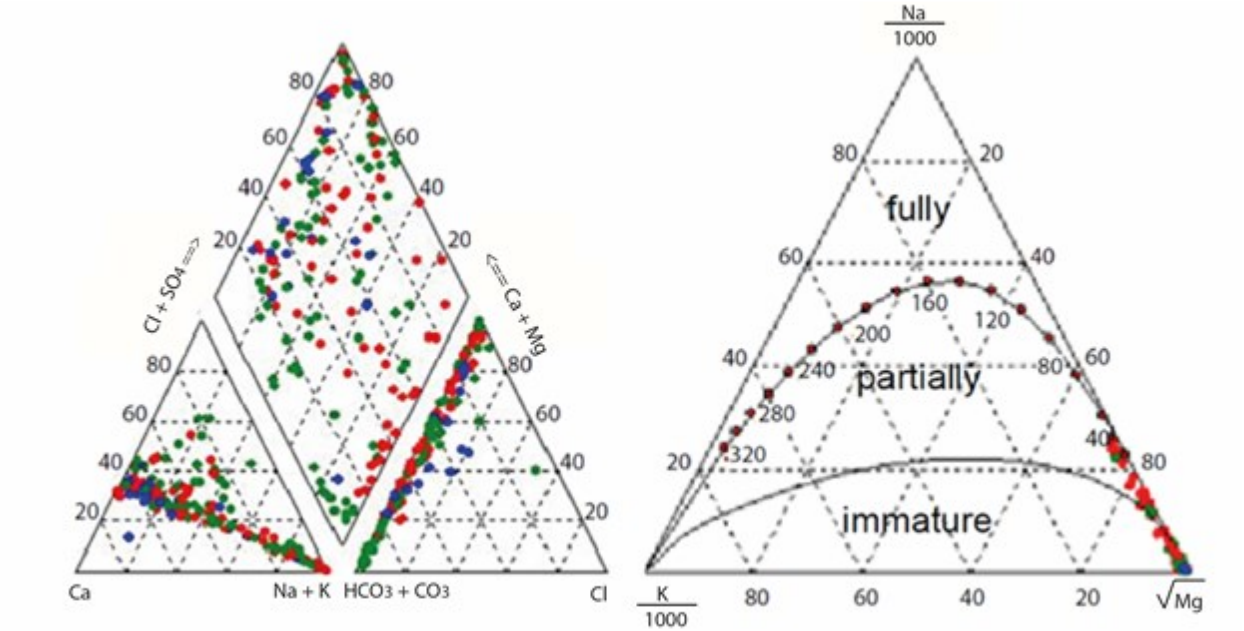

Figure 4: Classification of the groundwater sampled from the study area. (a) Piper diagram. (b) Giggenbach diagram. The red, blue, and green symbols represent groundwater samples collected in the central, western, and eastern regions, respectively.

Table 3.

EAST	Na-K		K-Mg		Na-K-Ca (B=4/3)
	TNKT80	TNKA83	TKMG88	TKM2F91	TNKCF73M
mean	182.3	119.0	37.0	15.0	123.9
median	172.0	109.5	36.0	11.0	127.0
S.D.	136.8	68.1	10.7	37.1	41.9
C.V.	0.8	0.6	0.3	2.5	0.3
CENTRAL	Na-K		K-Mg		Na-K-Ca (B=4/3)
	TNKT80	TNKA83	TKMG88	TKM2F91	TNKCF73M
mean	162.0	121.7	34.6	28.0	103.0
median	105.0	107.5	32.0	26.0	106.0
S.D.	167.9	62.7	12.8	56.7	49.5
C.V.	1.0	0.5	0.4	2.0	0.5
WEST	Na-K		K-Mg		Na-K-Ca (B=4/3)
	TNKT80	TNKA83	TKMG88	TKM2F91	TNKCF73M
mean	290.1	170.5	24.5	66.0	74.1
median	227.5	178.0	24.0	63.5	112.0
S.D.	206.0	54.9	6.9	35.9	63.9
C.V.	0.7	0.3	0.3	0.5	0.9

Temperatures calculated (°C) from hydrochemical results using the geothermometer relations.

4.2 Temperature Calculation

The temperature estimates have significant differences in the results from each geothermometer used. We hypothesize that these errors could be related to the precision and accuracy of the chemical analyses, contamination of the samples, and varied geological setting used for the formulas. However, the results presented in this work may be considered representatives in terms of the regional trend.

Table 3 compiles the temperatures calculated from the hydrochemical database using geothermometer equations (Table 2). Figure 5 shows a high statistical dispersion of temperature values. The Na-K geothermometers, TNKT80 (Tonami, 1980) and TNK2A83 (Arnorsson et G., 1983), generally show the highest values. The Na-Ca-K geothermometer, TNKCF73M (Fournier and Truesdell, 1973), exhibits its highest mean values in the eastern block. The western zone presents the higher temperatures for the Na-K geothermometers, with an average of 290.1 °C and 170.5 °C, respectively. The K-Mg geothermometers, TKMG88 (Giggenbach, 1988) and TKM2F91, shows the least correlation with values that are contradictory. Through this initial approach, it is easy to distinguish two groups wherein the average temperatures are over and below 100 °C.

The total error propagation has two components, one mathematical and the other, analytical. Previous authors have developed coefficients of variance with respect to an ideal tendency that gives an approximation to the mathematical error between the observed (direct measurements for this study were unavailable) and inferred temperatures. Due to this, we evaluate the geothermometers given by the Solgeo software (Verma et al., 2008) with their respective error propagation (Díaz et al., 2008; Bevington, 2003; Sprinthall, 2011; Fournier, 1979; Verma and Santoyo, 1997; Truesdell, 1976; Verma et al., 2006). This helped determine the most appropriate geothermometer, in accordance with the trends proposed by Fournier , 1979, Verma, 1997 and (Díaz et al., 2008; Bevington, 2003; Sprinthall, 2011; Fournier, 1979; Verma and Santoyo, 1997; Truesdell, 1976; Verma et al., 2006). The source of error used was the real uncertainty of the geochemical analysis (Table 1 and Appendix A).

4.3 Principal Component Analysis (PCA)

A multivariate statistical analysis was performed to determine patterns, trends, and similarities between the physicochemical parameters and estimated temperatures. The XLSTAT software was used for this data assessment. Figure 5 shows the contribution degree of variances and factors based on eight physicochemical parameters and the relationship between different geothermometers. A Principal Component Analysis (PCA) was used to explain the relationship between the factors affecting the obtained temperatures (Davis, 2002).

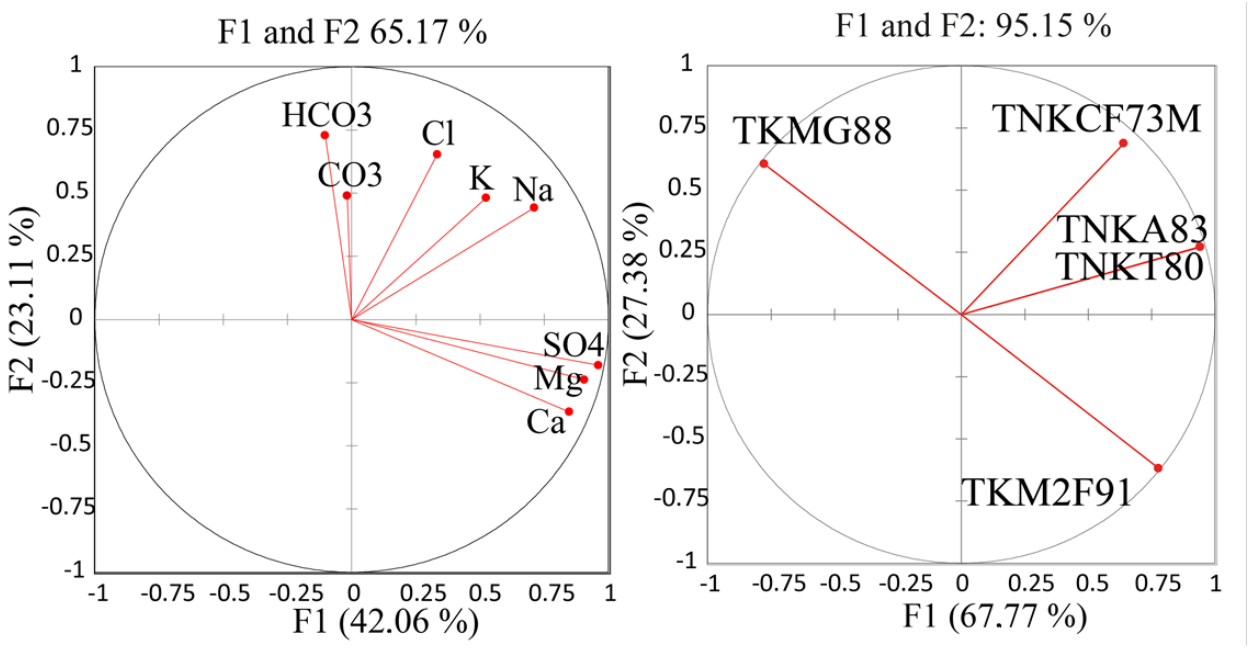

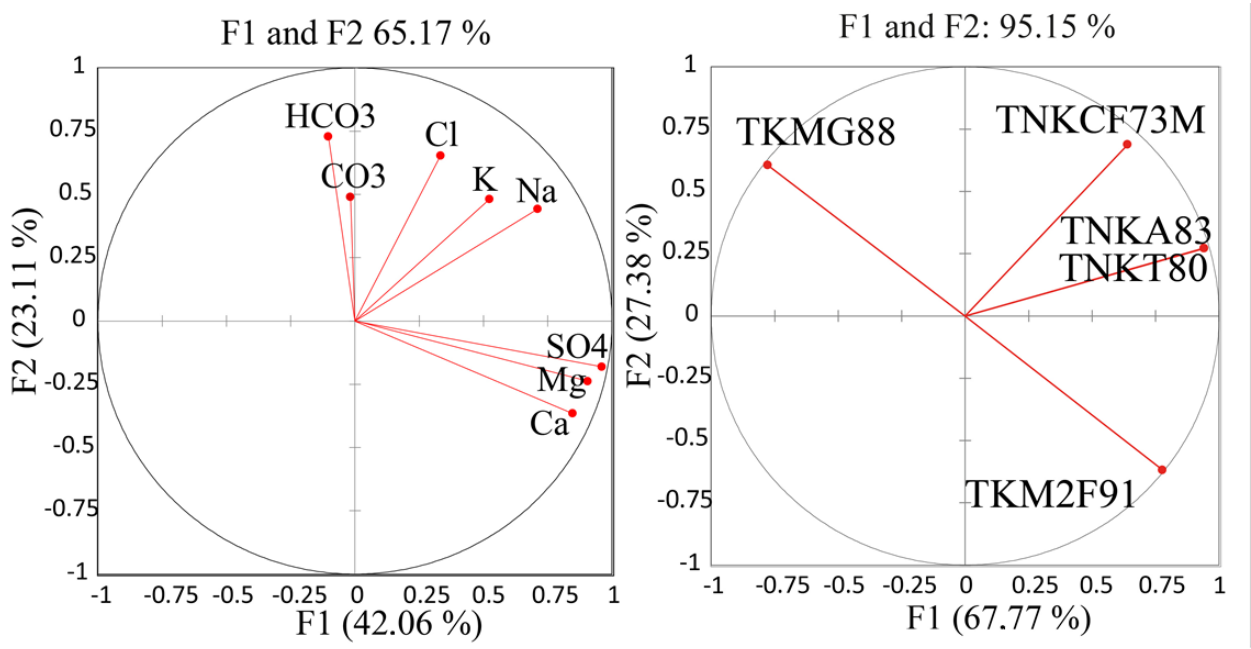

Figure 5: Principal Component Analysis for (a) the hydrogeochemical parameters, and (b) the temperature of geothermometers used throughout the Eastern Cordillera Basin. TNKT80 (Tonami, 1980), TNK2A83 (Arnorsson et al., 1983), TKM2F91 (Fournier-2, 1991), TKMG88 (Giggenbach, 1988), and TNKCF73M (Fournier and Truesdell, 1973).

The physicochemical parameters describe a function (F_1) with a 42.06% correlation between variances and factors, revealing a high loading of SO_4, Mg and Ca (Figure 5a). The function F_2, equaling 23.11% of the data, shows an adverse correlation between Na and the other elements. Function F_3 explains only 14.49% of the variance, therefore the values on this axis are not reliable. The Cl and CO_3 values have no correlation with any other component. The calculated temperatures are shown in Figure 5b with F_1 equal to 67.77%, indicating a high positive correlation for TNKA83 and TNKT80. The F_1(67.77%) and F_2(27.38%) exposes a null correlation between the TKMG88 and TKM2F91. The TNKCF73M has no correlation with any of the other geothermometers.

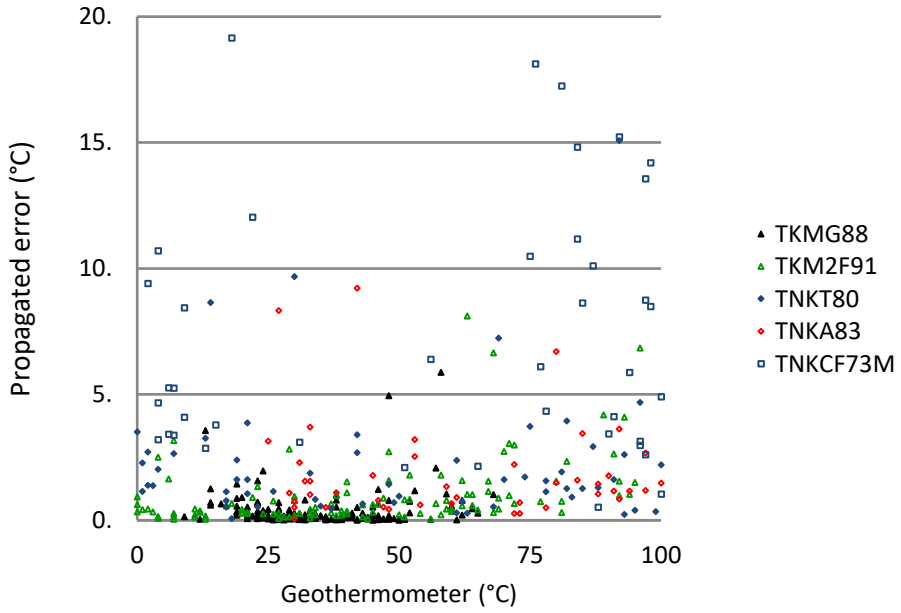

Figure 6: Plot showing the propagated error as a function of the temperature estimated by each geothermometer: TKMG88 (Giggenbach, 1988), TKM2F91 (Fournier-2, 1991), TNKT80 (Tonami, 1980), TNK2A83 (Arnórsson-1, 1983), and TNKCF73M (Fournier and Truesdell, 1973).

These physicochemical parameters highlight different temperature trends. However, according to the low dispersion of error propagation within the Giggenbach (1988) temperatures, as well as the high loading of Mg observed from the PCA (Figure 6), we consider this geothermometer as the best tool for the estimation of temperatures in the study area.

4.4 Geothermal gradient

We considered the depths from which all water samples were collected, and used an average (0.76 km) as the representative depth. Furthermore, we used geothermic information obtained from oil wells (Vargas, 2009) to constrain reliability of the temperature results and approximate the gradients according to observations in the study area. Because groundwater samples were collected close to coal beds, we have hypothesized that around these depths the waters were also ionically saturated under in-situ conditions. However, these waters may ascend to the surface through the many faults and fractures observed in the area, introducing a broad range of probable depths of provenance and ion saturation.

Using a maximum depth and the variety of temperatures estimated using the K-Mg geothermometer, the range of geothermal gradient values may fluctuate between 15 and 43 °C/km. Previous studies in this zone calculated geothermal gradients in the range of 32 to 50 °C/km, using information directly from oil wells (Vargas, 2009). Consequently, we recommend the TKMG88 geothermometer (Giggenbach, 1988) as the most appropriate for the estimation of the geothermal gradient in this region.

Figure 7 shows an interpolation of the geothermal gradient values estimated using the TKMG88 geothermometer. The map suggests high values towards the north-east, that are consistent with increases in the concentration of ions such as K, Na, and HCO_3. Though the interpolation could bias geothermal gradient patterns, we can infer a contrasting and colder area towards the west of the basin which does not see an anomalous increase in ion concentrations.

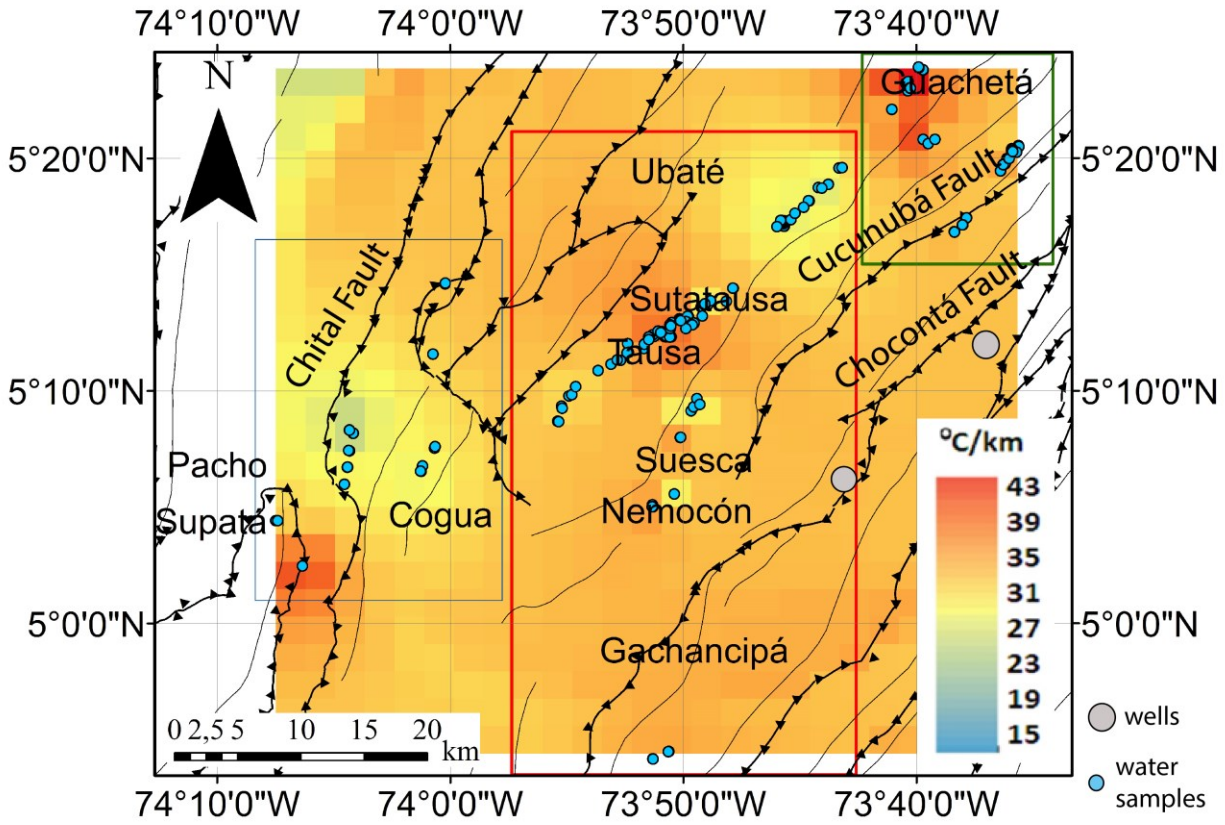

Figure 7: Geothermal gradients (°C/km) in the study area. The gray circles represent oil wells where Vargas et al. (2009) reported values of 45 °C/km.

4.5 Geotectonic implications

Datasets collected for this project are perpendicular to a hypothetical lithospheric tear zone, associated with a high geothermal anomaly region (Vargas et al., 2013). In this region, it is possible that the Adakite melts could have migrated from the upper mantle through the Caldas Tear, promoting the anomalous geothermal values (see Figures 7 and 8). We hypothesize that at least three geothermal anomalies highlighted in the study area (close to the localities of Gachetá in the NW, Tausa in the central region, and Supatá in the SW) may be related to magmatic bodies emplaced along a broader area of influence of the Caldas Tear.

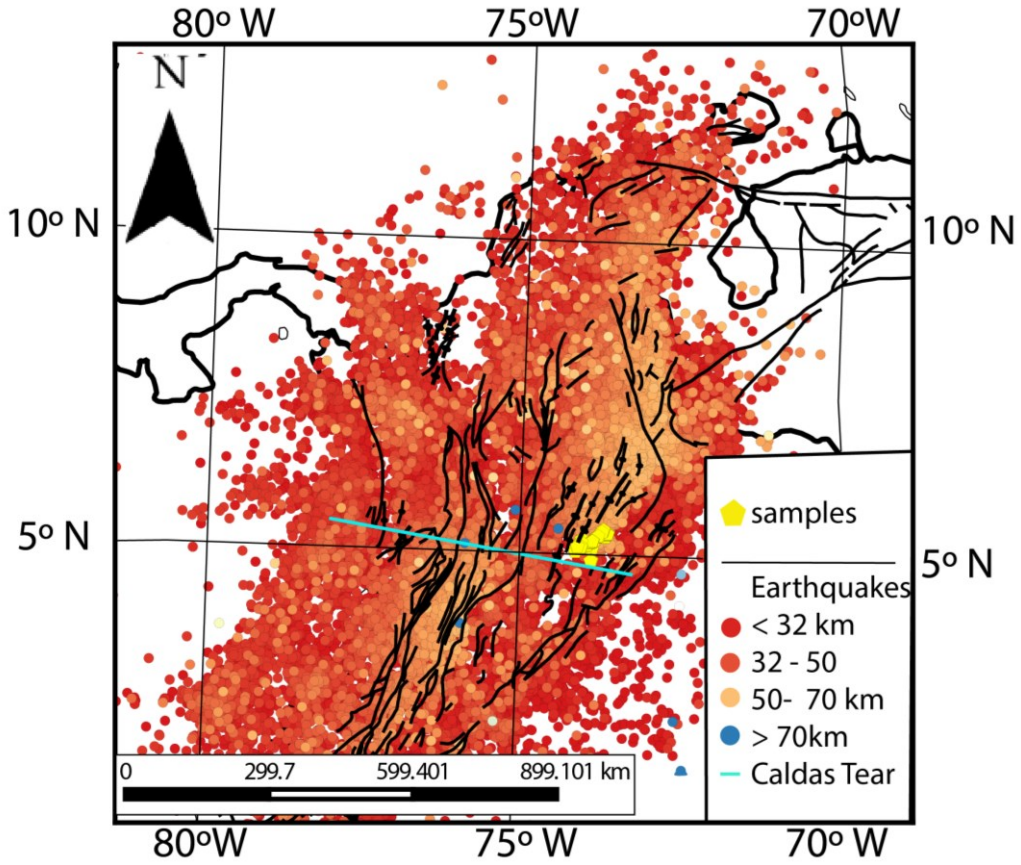

Figure 8: Seismicity in the study area (indicating a hypothetical lithospheric tear zone) and the location of samples.

5. CONCLUSIONS

We have analyzed the physicochemical parameters for 170 groundwater samples collected from coal mines in the Eastern Cordillera Basin of Colombia. In-situ groundwaters are mainly sulfated. They have a significant bicarbonate contribution and an almost negligible chloride contribution. A Principal Component Analysis (PCA) was used to detail the relationship between 12 selected variables and highlight the factors affecting geothermometers and the hydrogeochemical evolution in aquifers.

Using the Giggenbach (1988) geothermometer (TKMG88) and assuming the maximum water sampling depth (in the coal mines of the basin) as a representative, we have estimated a geothermal gradient map which shows values ranging between 15 and 43 °C /km, consistent with previous studies performed in the study area. The map identifies three anomalously high values. A possible explanation for the thermal anomalies could be the spatial proximity to a hypothetical lithospheric tear zone and fault systems. The geothermometer with the least error propagation was the TKMG88. Increased measurements from the zonal depth at which the methodology was calibrated, could help improve future results. . Certain failure structures such as faults and fractures in zones of varying lithology could also help in the selection of an appropriate geothermometer.

ACKNOWLEDGEMENTS

We are very grateful to the Universidad Nacional de Colombia for their collaboration during the research project developed by C.A. Barrera and J.E. Cortes. We also thank the Research Group of Geophysics for their support in this work, and the ANH-Antek S.A.S. for generously providing the data. Partial funding for this work was provided by Colciencias grants 12455218627/784-2011, 123356935004/0361-2013, FP44842-006- 2016, and 50491-2016. We value the assistance of the reviewers and the Editorial Office of Geodesy and Geodynamics to better the manuscript.

REFERENCES

1. [1]Díaz-González L., Santoyo, E., Reyes-Reyes, J.,: Tres nuevos geotermómetros mejorados de Na/K usando herramientas computacionales y geoquimiométricas: aplicación a la predicción de temperaturas de sistemas geotérmicos, Revista Mexicana de Ciencias Geológicas, V. 25, núm 3, (2008), 465-482.
2. [2]Yock, A.,: Geothermometry, Short Course on surface exploration for geothermal resources, El Salvador, (2009).
3. [3]Rolon, L. Lorenzo, J., Lowrie, A., and Barrero, D.,: Thrust, kinematics and hydrocarbon migration in the Middle Magdalena Basin, Colombia, South America, 21st Annual GCS-SEPM Conference, Houston, USA, (2001).
4. [4]Pedraza, F., and Mariño, M.,: Thermal evaluation of 6 wells of the central part of the Eastern Cordillera (Colombia) from paleogeotherms: implications on thermal history and hydrocarbons, Ingeniería y competitividad, v. 18, (2016) , 09-21.
5. [5]Hubach, E.,: Contribución a las unidades estratigráficas de Colombia, Servicio Geológico Nacional, Informe 1212, (Mscr.), Bogotá, Colombia, (1957), 1-166.
6. [6]Sarmiento, G,.: Visión regional de la Formación Guaduas.-Publicaciones Geológica, Especiales 20, INGEOMINAS, Bogotá, (1994), 165-180.
7. [7]Montoya, D., and Reyes, G.,: Geología de la plancha 209 Zipaquirá, Ingeominas, Bogotá, Colombia, (2003).

8. [8]Sarmiento, L.F.,: Mesozoic rifting and Cenozoic basin inversion history of the Eastern Cordillera, Colombian Andes, Inferences from tectonic models: Bogotá, ECOPETROL-Netherlands Research School of Sedimentary Geology, (2001), 295.
9. [9]Etayo, S,.: El Sistema Cretáceo en la región de Villa de Leiva y zonas próximas, Geología Colombiana,(1968).
10. [10]Pérez, G., and Salazar, A.,: Estratigrafía y facies del grupo Guadalupe, Geología Colombiana, Universidad Nacional de Colombia, Bogotá, Colombia, (1978).
11. [11]Fabre, A.: Dinámica de la sedimentación Cretácica en la región de la Sierra Nevada del Cocuy (Cordillera Oriental de Colombia), En: Proyecto Cretácico, Publicación Geológica Especial INGEOMINAS No. 16. Bogotá, (1985), XIX-1 a XIX-20.
12. [12]Acosta, J., and Ulloa, C.,: Mapa geológico del Departamento de Cundinamarca, Memoria explicativa, INGEOMINAS, Bogotá, Colombia, (1997).
13. [13]Guerrero, J.,: A Proposal on the Classification of Systems Tracts: Application to the Allostratigraphy and Sequence Stratigraphy of the Cretaceous Basin, Part 2: Barremian to Maastrichtian, Geologia Colombiana, No 27, Pgs. 27 - 49, Bogotá, Colombia, (2002).
14. [14]Sarmiento, G.,: Estratigrafía y Medio de Depósito de la Formación Guaduas, Boletín Geológico, Ingeominas, vol. 32, no. 1-3, (1992), 3-44.
15. [15]Guatame, C., and Sarmiento, G.A.,: Interpretación del Ambiente Sedimentario de los Carbones de la FormaciónGuaduas en el Sinclinal Checua-Lenguazaque aparir del análisis petrográfico, Geologia Colombiana, No 29, Bogotá, Colombia, (2004), 41-57.
16. [16]Mejía-Umaña, L.J., Convers-Gómez, C.E., and González-Casallas, J.F.,: Coal Microlithotype analysis of the Guaduas Formation in the Sueva Synncline, Cundinamarca, Geología Colombiana, v. 31, Bogotá, (2006) ,11-26.
17. [17]Etayo, Serna, F.: Zonation of the Cretaceous of Central Colombia by Ammonites, Publ Esp del Ingeominas No 2, INGEOMINAS, Bogotá, Colombia, (1979), 1-186.
18. [18]Guerrero, J., Sarmiento, G., Navarrete, R: The Stratigraphy of the W Side of the Cretaceus Colombian Basin in the Upper Magdalena Valley, Reevaluation of selected areas and localities including Aipe, Guaduas, Ortega and Piedras, Geología Colombiana, No 25, Bogotá, Colombia, (2000), 45-110.
19. [19]Ulloa, C. y Acosta, J.,: Geología de la Plancha 208-Villeta, Informe Interno I-2200, INGEOMINAS, Bogotá, Colombia, (1993), 118.
20. [20]Cáceres, C., Etayo, F.,: Bosquejo Geólogico de la Región del Tequendama, I Congreso Colombiano de Geología, Opúsculo guía, Excursión pre-congreso 22, Bogotá, Colombia, (1969).
21. [21]Hubach, E,.: Aspectos geologico-petrolíferos de Colombia en 1951, INGEOMINAS, (1951).
22. [22]Renzoni, G.,: Apuntes acerca de la litología y ectónica de la zona al este y sureste de Bogotá, Boletin geológico 10(1-3),Servicio Geológico Nacional, Bogotá, (1963), 59-79.
23. [23]Guerrero, J., and Sarmiento, G.,: Estratigrafía Física, Palnológica, Sedimentológica y Secuencial del Cretácico Superior y Paleoceno del Piedemonte Llanero. Implicaciones en Exploración Petrolera,-Geología Colombiana, n. 20, Bogotá, (1996), 3-66.
24. [24]ANH-Antek, : Caracterización hidrogeológica e hidrogeoquímica de las áreas con potencial para yacimientos no convencionales de hidrocarburos tipo coalbed methane, Bogotá, Colombia, (2015).
25. [25]Antek S.A.,: ISO 17025 Quality Assurance Manual for Environmental and Geochemical Analysis, Bogotá, Colombia, 2009.
26. [26]APHA, AWWA, WEF,: Standard Methods for the Examination of Water & Wastewater, 22st ed. (2012).
27. [27]Prasanna, M.V., Chidambaram, S., Shahul Hameed, A., Srinivasamoorthy, K.,: Study of evaluation of Groundwater in Gadilam basin using hydrogeochemical and isotope data, Environ. Monit. Assess., 168, (2010), 63- 90.
28. [28]Chidambaram, S., Prasanna, M.V., Singaraja, C., Thilagavathi, R.,: Study on the Saturation Index of the Carbonates in the Groundwater Using WATEQ4F in Layered Coastal Aquifers of Pondicherry, J. Geological Society of India, 80, (2012), 813-824.
29. [29]Waterloo Hydrogeologic,: AquaChem. Water Quality Analysis & Geochemical Modeling, www.waterloohydrogeologic.com/aquachem/ (2010).
30. [30]ESRI, Inc.: Arc-GIS, www.esri.com, (2010).
31. [31]Addinsoft : XLSTAT version 14.0.0.162. Multivariate Statistical Analysis, www.xlstat.co, (2015).
32. [32]Verma et al.,: SolGeo: A new computer program for solute geothermomters and its application to Mexican geothermal fields, Geothermics, Scence Direct, (2008).
33. [33]Abdel-Lattif, A., and El Kashouty, M.,: Statistical Investigation of the groundwater system in Darb El- Arbaein, Southwestern desert, Egypt, Earth Sci. Res. J. 13 (2), (2009), 166-182.
34. [34]Brindhla, A.K., Elango, L.,: Hydrochemical characteristic of groundwater for domestic and irrigation purposes in Madhuranthakam, Tamil Nadu, India, Earth Sci. Res. J. Vol. 15 (2), (2011), 101- 108.
35. [35]Verma P.,: Thermodynamic classification of vapor and liquid dominated reservoir and fluid geochemical parameter calculations, Geofísica internacional, Universidad Nacional Autónoma de México, México Distrito Federal, v. 36, (1997).
36. [36]Bevington, P. and Robinson, D.: Data reduction and error analysis for the Physical Sciences, Third edition, ISBN 0-07 247227-8, (2003).
37. [37]Vargas, C.A. Alfaro, C. Briceño, L.A. Alvarado, I. and Quintero, W.,: Mapa Geotérmico de Colombia. X Simposio Bolivariano Exploración Petrolera en Cuencas Subandinas, Colombia, (2009).
38. [38]Cortes, J.E., Muñoz, L., Gonzalez, C.A., Nino, J.E., Polo, A., Suspes, A., Siachoque, S.C., Hernandez, A., Trujillo, H.,: Hydrogeochemistry of the formation waters in the San Francisco field. UMV Basin, Colombia –a multivariate statistical approach-, Journal of Hydrology, 539, (2016), 113-124.
39. [39]Méndez, B.A.,: Geoquímica e Isotopía de Aguas de Formación (Salmueras Petroleras) de Campos Mesozoicos de la Cuenca Sureste de México: Implicación en su Origen, Evolución e Interacción Agua- Roca en Yacimientos Petroleros, Tesis Doctoral en Geociencias. Universidad Nacional Autonoma de Mexico, Ciudad de Mexico, Mexico, (2007).
40. [40]Cortes, J.E., Arboleda, G., Sepúlveda, V., Piragáuta, N., Higuera, O., Castro, A.,: Hydrogeological and Hydrogeochemical evaluation of Groundwaters and Surface Waters in Potential Coalbed Methane Areas in Colombia, Submitted for publication to Journal of Coal Geology, (2017).
41. [41]Bello, O.A., Ozgur, N.,Caliskan, T.A.: Hydrogeological, hydrogeochemical and isotope geochemical features of thermal waters in simav and environs. In: Proceedings of Thirty-Ninth Workshop on Gothermal Reservoir Engineering, Stanford University, California, February 24-26. SPT-TR-202, (2014).

42. [42]Hounslow, A.,: Water Quality Data: Analysis and Interpretation, Taylor & Francis Inc. 1 edition, Bosa Roca, United States, (1995).
43. [43]Tonami, F.,: Some remarks on the application of geochemical techniques in geothermal exploration, in Proceedings of Advances in European Geothermal Research, 2nd Symposium: Strasbourg, (1980), 428-443.
44. [44]Arnorsson, S., Gunnlaugsson, E., and Svavarsson, H.,: The chemistry of geothermal waters in Iceland II, Mineral equilibria and independent variables controlling water compositions, Geochimica et Cosmochimica, (1983), 547-566.
45. [45]Fournier, R., and Truesdell, H.,: An empirical Na-K-Ca geothermometer for natural waters, Geochim, Cosmochim, Acta. 37, (1973), 1255-1275.
46. [46]Giggenbach, W.F.,: Geothermal solute equilibria, Geochimica, Cosmochim, Acta. 52, (1988), 2749 – 2765.
47. [47]Sprinthall, R. C.,: Basic Statistical Analysis, 9th Edition: Pearson, (2011).
48. [48]Fournier, R. O.,: A revised equation for the Na/K geothermometer, Geothermal Resources Council, Trans. 3, (1979), 221-224.
49. [49]Verma, and Santoyo.,: New improved equation for Na/K and SiO2 geothermometers by error propagation, Mexico, (1997).
50. [50]Truesdell, A. H.,: Summary of Section III - geochemical techniques in exploration, Proceedings of the 2nd U.N. Symposium on the Development and Use of Geothermal Resources, San Francisco, USA, (1976).
51. [51]Verma et al.,: Applicaton of the error propagation theory in estimates of static formation temperatures in geothermal and petroleum boreholes, Energy Conversion & Management, ScienceDirect, (2006).
52. [52]Davis, J.C.,: Statistics and Data Analysis in Geology, 3rd Edition, Kansas Geological Survey, (2002).
53. [53]Vargas, C.A., Mann, P.,: Tearing and Breaking Off of Subducted Slabs as the Result of Collision of the Panama Arc-Indenter with Northwestern South America, Bulletin of the Seismological Society of America, v. 103, No 3. pp 2025-2046, (2013).
54. [54]Fournier, R.O.,: Water geothermometers applied to geothermal energy. In: Verma et al.,: SolGeo: A new computer program for solute geothermomters and its application to Mexican geothermal fields, Geothermics, Scence Direct, (2008).

APPENDIX A

Bevington (1969) proposed the following equation, known as the error propagation equation.

$$\sigma_x{}^2 = \left((\sigma_u{}^2) \left(\frac{\delta x}{u}\right)^2 \right) + \left((\sigma_v{}^2) \left(\frac{\delta x}{v}\right)^2 \right) + \left((\sigma_n{}^2) \left(\frac{\delta x}{n}\right)^2 \right) + \cdots$$

Where, $x = f(u, v, n, \ldots)$.

The equation used to estimate the error propagation for Na-K geothermometers is:

$$\sigma_t = \left(\frac{B}{A + \log\left(\frac{Na}{K}\right)} \right) \cdot \left(\frac{S_B{}^2}{B^2} + \frac{\frac{1}{\ln(10)^2}\left(\frac{(s_{Na}{}^2)}{Na^2} + \frac{(s_K{}^2)}{K^2}\right) + s_A{}^2}{\left(A + log\left(\frac{Na}{K}\right)\right)^2} \right)^{\frac{1}{2}}$$

If the original equation for Na-K has the form

$$t(°C) = \frac{B}{A + log\left(\frac{Na}{K}\right)} - 273.15$$

The equation used for the estimation of error propagation for K-Mg geothermometers is:

$$\sigma = \frac{B}{\left(log\left(\frac{K^2}{Mg}\right) + A\right)^2} \cdot \left(s_A{}^2 + \frac{s_B{}^2}{B^2 . \left(log\left(\frac{K^2}{Mg}\right) + A\right)^2} + \left[\frac{1}{\ln(10)^2} \left(\frac{s_K{}^2}{K^2} + \frac{s_{Mg}{}^2}{Mg^2} \right) \right] \right)^{\frac{1}{2}}$$

If the original equation for K-Mg has the form

$$t(°C) = \frac{B}{A + log\left(\frac{K^2}{Mg}\right)} - 273.15$$

The equation used to estimate the error propagation for Na-K-Ca geothermometers is:

$$\sigma = \frac{A}{\ln(10)\left(log\left(\frac{Na}{K}\right) + B\left(log\left(\frac{\sqrt{Ca}}{Na}\right) + C\right) + D\right)^2} \cdot \left(\frac{s_{Na}{}^2 (1-B)^2}{Na^2} + \frac{s_k{}^2}{K^2} + \frac{B^2 s_{Ca}{}^2}{4Ca^2} \right)^{\frac{1}{2}}$$

If the original equation for Na-K-Ca has the form:

$$t(°C) = \frac{A}{log\left(\frac{Na}{K}\right) + B\left[log\left(\frac{\sqrt{Ca}}{Na}\right) + C\right] + D} - 273.15.$$

Though our estimations incorporate uncertainties for the elements evaluated (Table 1), another source of error related to the coefficients A, B, C, and D (unknown from some used equations), may increase the total uncertainty throughout the calculations.